REVIEW

VIEW

Theranostics for MRI-guided therapy: Recent developments

Ziwei Zhang[1,2] | **Feng-Lei Zhou**[3,4] | **Gemma-Louise Davies**[2] | **Gareth R. Williams**[1] ●

[1] UCL School of Pharmacy, University College London, London, UK

[2] UCL Department of Chemistry, University College London, London, UK

[3] Department of Medical Physics and Biomedical Engineering, University College London, London, UK

[4] College of Textiles and Clothing, Qingdao University, Qingdao, PR China

Correspondence

Gareth R. Williams, UCL School of Pharmacy, University College London, 29–39 Brunswick Square, London WC1N 1AX, UK

Email: g.williams@ucl.ac.uk

Abstract

Recent advances in bioimaging, biochemistry, and bioinformatics have facilitated the development of personalized and precision medicine. Theranostics, combining imaging modalities and therapeutic agents, have garnered a lot of attention in this context, owing to their potential to monitor and control treatment for individual patients. A promising strategy to achieve this goal involves the development of therapy guided by magnetic resonance imaging (MRI). MRI has a high degree of soft tissue contrast, low invasiveness, high depth of penetration and good spatial resolution. MRI-guided therapy could thus allow precise and time-resolved assessment of disease conditions and therapeutic progression. This article will give a brief introduction to the principles of MRI, and describe recently developed strategies to produce MRI-guided therapies. A number of theranostics based on T_1, T_2, or chemical exchange saturation transfer (CEST) MRI have been explored to track the route of drug carriers in vivo and image diseased tissue so as to enhance bioavailability, overcome complex delivery barriers, and assess therapeutic responses. In addition, the integration of thermal therapy and MRI imaging offers a strategy to noninvasively identify target areas, plan treatment, and provide real-time assessment of the efficacy of tumor ablation. We also discuss advances in intelligent nanoparticles combining small molecule drugs, thermal treatment and multimodal imaging, arguing that these multifunctional agents can further improve therapeutic outcomes.

1 | INTRODUCTION

New insights into molecular pathology have made a huge difference to the range of therapies available to clinicians over the last few decades, culminating in the recent emergence of personalized and precision medicine.[1,2] A large variety of targeted therapies have been reported, and some have already been approved by the Food and Drug Administration (FDA).[3,4] However, new concerns arise with these formulations because traditional pharmacokinetics studies measure plasma drug concentrations and do not reflect the local concentration of therapeutic agents delivered to the target areas.[5,6] In addition, for the development of effective personalized medicine, it is important to image the disease condition and monitor the therapeutic effect as a function of time. As a result, there is a need to develop novel approaches to precisely assess the progression of a disease and monitor drug delivery in vivo. Real-time

Abbreviations: CEST, Chemical exchange saturation transfer; MRI, Magnetic resonance imaging; PAI, Photoacoustic imaging; PDT, Photodynamic therapy; PTT, Photothermal therapy

monitoring of therapeutic outcomes can help to track and tailor drug doses in a timely and accurate manner for patients, allowing adjustments of the applied doses in order to keep the concentration within the therapeutic window. Reliable in vivo drug release information and assessment of disease progression can not only help to reduce side effects but also increase therapeutic efficacy.

One strategy to achieve this goal is theranostics. In essence, the term "theranostics" refers to the integration of imaging and therapy, very often based on the use of micro and nanosized carriers. Taking advantage of molecular imaging agents, theranostics provide tantalizing potential for tracking therapeutic agents in vivo.[7] In clinical practice, theranostics are often labeled or packaged with imaging and therapeutic agents, aiming for noninvasive assessment of local disease progression, quantification of carrier accumulation, and drug release.[8] This is particularly useful in the treatment of cancer or central nervous system (CNS) diseases, where drug delivery faces challenges owing to narrow therapeutic indices, high renal clearance, complicated physiological barriers and susceptibility to multidrug resistance. Theranostics can be envisaged with a number of attractive features, including high loading capacity, long blood circulation times, selective accumulation at disease sites, or targeting particular molecular alterations.[9] In some cases, controlled/triggered release of therapeutic agents is preferable in order to better control the therapeutic outcome. In an ideal scenario, theranostics would give enhanced biodistribution of an active agent, allow a predictable therapeutic outcome, and improve therapeutic effects with minimized side effects.[10]

There exists a wide variety of biomedical imaging modalities; among these, magnetic resonance imaging (MRI) stands out because of its high degree of soft tissue contrast, minimal invasiveness, depth of penetration, and spatial resolution.[11,12] MRI works by detecting the relaxation times of protons in endogenous molecules such as water, lipids, and proteins.[13] In many cases, exogenous contrast agents (CAs) are required to enhance the quality of MRI images and permit accurate diagnoses to be made. CAs work to improve MRI contrast by affecting the local relaxation behavior of protons. CAs can be incorporated into theranostics to provide detailed information about drug release and delivery. In 2020, a first-in-human trial was reported using MRI-guided nanoparticle theranostics, which can be used to image brain tumor metastases in patients, as well as quantify the local drug concentration.[14] A follow-on Phase II clinical trial is ongoing. This offers strong proof of the potential of MRI-guided nanotheranostics in precision medicine. In this review article, we will focus on recent progress made in the engineering of MRI-based theranostics to engender in vivo spatiotemporal tracking of active agents and deliver therapeutic effects with high image contrast.

2 | MRI THEORY

MRI functions by making use of the nuclear magnetic resonance (NMR) effect. In response to a strong external magnetic field (B_0), spin-active nuclei disequilibrate and subsequently reequilibrate to their original state at a particular frequency (R_F). This motion is described as Larmor precession (ω; Equation 1), which is linearly related to the applied magnetic field strength (B_0) and the gyromagnetic ratio of the nucleus (γ).

$$\omega = -\gamma \times B_0 \text{rad} s^{-1}. \tag{1}$$

When R_F (often induced by an oscillating electromagnetic field B_1 perpendicular to B_0) is applied, motions of net magnetization vectors (the sum of the total magnetic moments of the individual nuclei with Larmor precession), change from a position parallel to B_0 to one transverse to it. Upon removal of the applied R_F, the nuclei then undergo a relaxation process to return to their original position through two mechanisms, known as longitudinal (spin–lattice) or transverse (spin–spin) relaxation.[13,15] In an MRI system, the relaxation process is repeated by application of a rapid series of spaced R_F pulses so as to generate electric signals from relaxing magnetic moments and obtain a time-dependent NMR signal. From this, the relaxation times (longitudinal, T_1, and transverse, T_2) can be derived based on Fourier transformation. Imaging signals are often generated by monitoring the corresponding longitudinal and transverse relaxation, which are spatially resolved electronically. The chemical and physical natures of tissues in the body result in variations in proton relaxation behavior, and thus in endogenous MRI contrast. Specifically, local variations in the water proton density caused by differences in the water, protein, and lipid concentrations lead to different T_1 and T_2 values. This allows tissues to be differentiated.[13,16]

Unfortunately, the low sensitivity of endogenous contrast in MRI is often not sufficient for diagnosis of a pathology of interest. Exogenous CAs are required in these circumstances to deliver better MR images, acting by locally shortening the T_1 and T_2 proton relaxation times. Typically, CAs contain paramagnetic species (e.g., Gd^{3+} and Fe^{2+} or Fe^{3+}) with unpaired electrons, and the corresponding magnetic moments engage in dipolar and scalar interactions with nearby water protons.[17] Subsequently, the local water protons relax immediately and quickly exchange positions with another unrelaxed water proton, therefore shortening the average relaxation times. Enhancement in contrast can be achieved when the targeted area possesses either higher vascularity for the CAs or the CAs have higher affinity for the target than other areas. This is often the case with diseased tissues; for instance, tumors differ from healthy tissues in terms of

metabolism and are more highly vascularized. This means they can take up CAs to a greater extent than healthy tissue, resulting in enhanced contrast in MR images.

The proton relaxivity (r), defined by Equation (2), relates to the efficiency of the CAs in terms of signal enhancement. The ability of the paramagnetic atoms in CAs to enhance the relaxation of endogenous protons is measured in terms of the change in relaxation rate ($\Delta 1/T_i$, $i = 1,2$) versus the millimolar concentration of paramagnetic agent or metal ion (mM).[18] Although most MRI CAs have effects on both T_1 and T_2, they are categorized as T_1 (usually paramagnetic complexes) or T_2 (mostly superparamagnetic iron oxides) agents according to whether their effects are more pronounced for T_1 or T_2.[19] T_1 CAs predominantly reduce the longitudinal relaxation time, giving rise to hyperintense signals in T_1-weighted images (bright contrast), while T_2 CAs (or negative CAs) primarily decrease T_2 of water protons in the regions they are delivered to, producing T_2-weighted images and darkening the region of interest.[19]

$$r_i = \frac{\Delta\left(\frac{1}{T_i}\right)}{[mM]} \quad i = 1, 2. \tag{2}$$

3 | THERANOTICS FOR MRI-GUIDED DRUG DELIVERY

MRI has been widely explored in personalized medicine to track the route of drug carriers in vivo and provide structural, functional, and molecular information about the tumor region. Here we will review the latest theranostic systems developed for codelivery of therapeutic agents and MRI CAs. These have been developed to improve bioavailability, overcome complex delivery barriers, assess therapeutic responses, and alleviate adverse effects.

3.1 | T_2-MRI

3.1.1 | Overcoming biological barriers

Physiological and pathological barriers challenge drug delivery. A number of MRI-traceable, targeted, theranostics have been designed to address this issue as well as providing real-time information on delivery route and corresponding therapeutic responses. For example, the blood–brain–barrier (BBB), which protects the brain from harmful pathogens, comprises a major biological barrier for drug delivery to the brain. Israel et al. have outlined various strategies to penetrate or enhance permeability across the BBB via nonspecific or active magnetic target-

ing using magnetic iron oxide nanoparticles (MNPs).[20] These strategies are particularly helpful in the treatment of solid tumors in the brain, such as glioblastoma (GBM). Ganipineni and coworkers reported poly(lactic-co-glycolic acid) (PLGA)-based nanoparticles loaded with paclitaxel (PTX) and superparamagnetic iron oxide nanoparticles (SPIONs) to treat GBM via magnetic targeting.[21] The BBB at the GBM site was seen to be disrupted based on MRI images, and PLGA nanoparticles could be accumulated in the mouse brain via magnetic treatment in an ex vivo biodistribution study. Efforts have also been made to use magnetic resonance–guided focused ultrasound (MRgFUS) to bypass the BBB. This approach works by using low energy ultrasound (US) to transiently disrupt the BBB, and can precisely target systemically delivered therapy to specific areas in the CNS.[22] Fan et al. fabricated microbubbles loaded with magnetic-labeled doxorubicin (SD-MBs) that could be accumulated in the brain tumors of glioma rats with the aid of both of focused US sonication and magnetic fields, as shown in US and T_2-weighted MRI images (Figure 1A–F).[23] Furthermore, the amount of doxorubicin (DOX) present could be quantified based on the T_2-weighted MRI signal, providing an advanced molecular therapy for antiglioma treatment as shown in Figure 1G–I. A recent trial on patients with amyotrophic lateral sclerosis demonstrated that MRgFUS can safely deliver agents to the target areas of the brain, as monitored by MRI.[23]

3.1.2 | Targeted delivery

MRI-guided theranostics for targeted therapy have been extensively explored, typically to treat cancer cells overexpressing particular receptors. Approaches targeting a single biomarker often reach a cell-binding plateau with a surface density below the saturation limit, resulting in a low therapeutic efficiency and increasing risks of off-target effect.[24] Hence, active receptor-targeting and magnetic-targeting strategies have been combined to enhance MRI detection and improve therapeutic efficacy.[25,26] A magnetic mesoporous silica nanoparticle coloaded with a redox-responsive DOX prodrug and the Arg–Gly–Asp (RGD) ligand was prepared by Chen and colleagues to improve active-targeting ligand-stimulated endocytosis with the aid of magnetic targeting.[25] The nanovehicles prepared were proven to be enriched at the target site as a result of the combined effect of active ligands and external magnetic targeting. Enhancement in T_2-weighted MRI images of a murine model bearing $\alpha v\beta 3$-integrin positive HeLa tumors was also seen. As a result, the combined approach led to better therapeutic outcomes than either the magnetic or biomarker-targeting strategy alone.
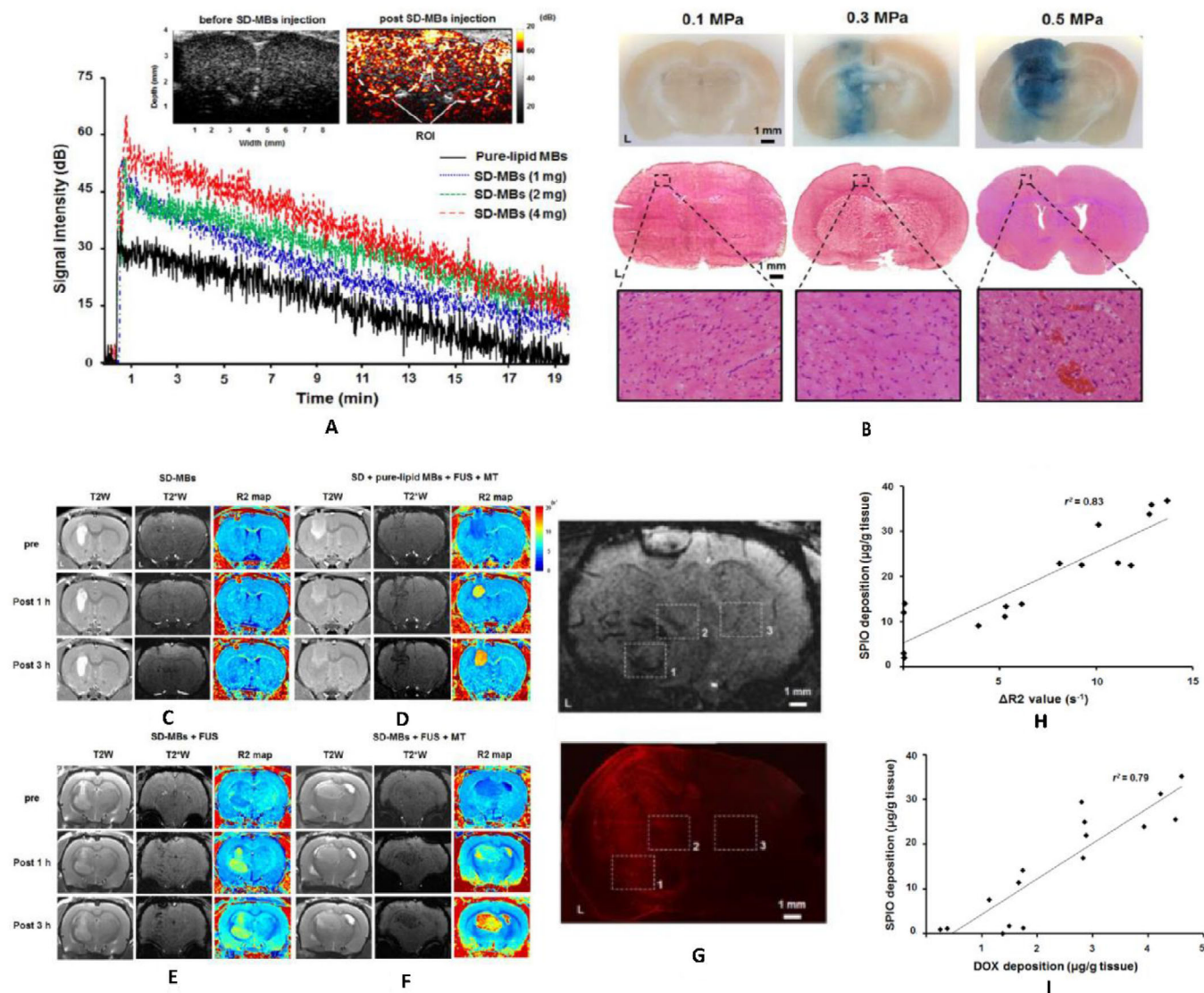
FIGURE 1 Acoustic performance of SD-MBs: (A) A plot showing enhancement in the US signal and in vivo lifetime with different SD payloads; (B) opening of the BBB via focused ultrasound (FUS) sonication (top: brain section; middle: corresponding hematoxylin-eosin staining; bottom: 200× magnification of hematoxylin-eosin staining). In vivo T_2-weighted MRI imaging (top: before treatment; middle: 1 h after treatment; bottom: 3 hours after treatment) for (C) SD-MB, (D) SD + MB + FUS + magnetic targeting (MT), (E) SD-MB + FUS, and (F) SD-MB + FUS + MT. (G) MRI image and corresponding fluorescent image reflecting the local magnetic-labeled DOX in the brain. Also shown are the correlations between (H) superparamagnetic iron oxide (SPIO) deposition and ΔR_2 values and (I) SPIO deposition and DOX accumulation. Reproduced with permission.[23] Copyright 2016, Ivyspring International Publishers

Similar work combining RGD and magnetic targeting was achieved with RGD conjugated magneto-vesicles (MVs) carrying DOX .[26] An in vivo study in mice showed that the MVs exhibited potent therapeutic efficacy because of the synergistic effect of active and magnetic targeting (Figure 2A–D). Researchers have also proposed a dual-receptor targeting strategy, which involves forming multivalent interactions between the drug-delivery vehicle and multiple membrane receptors before the former enters host cells. For example, Shen et al. developed RGD and GX1-peptide-conjugated magnetic poly-L-lysine MNPs carrying DOX.[27] It was demonstrated that this dual-ligand

MRI probe efficiently binds to vascular endothelial growth factor and integrin receptors and inhibits the growth of tumors in vivo more effectively than nanoprobes targeting a single receptor.

Another targeting strategy is to coat theranostic particles with cell-based membranes. This can allow targeting to cancer cells and alleviate losses from nonspecific uptake by the immune system.[28] Various cells such as human platelets[29] or leukocytes[30] have been used as a source of membrane material. A study by Zhu and coworkers explored a number of different types of cracked cancer cell membranes (CCCM) as a shell coating DOX-loaded
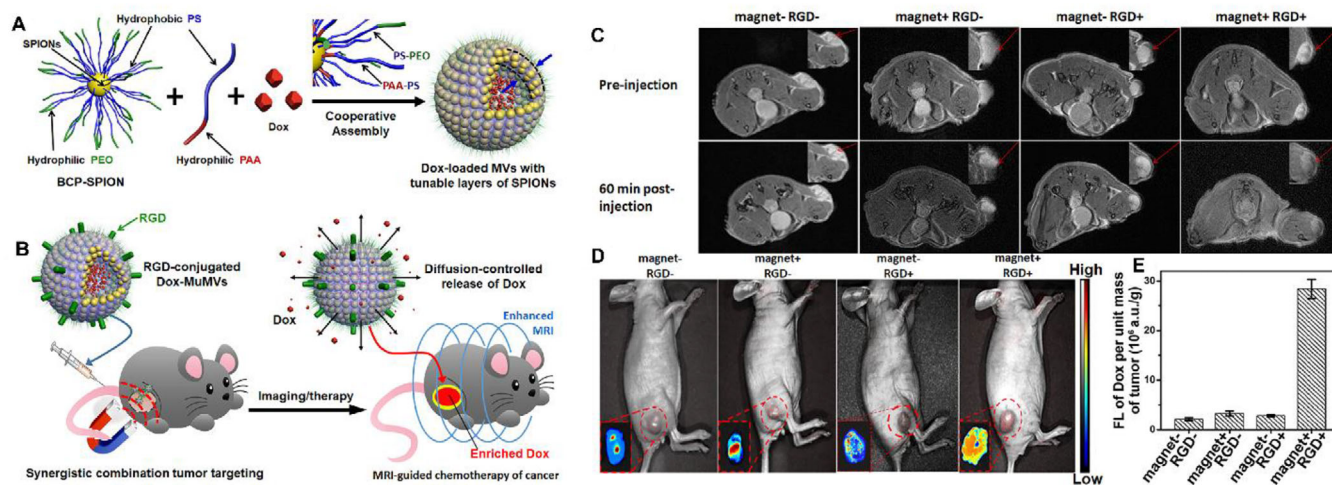
FIGURE 2 Schematics showing (A) the fabrication of RGD-conjugated MVs loaded with DOX (RGD–MVs–DOX) and (B) the utilization of RGD–MVs–DOX for T_2 MRI-guided magnetic delivery of DOX into tumor-bearing mice. (C) In vivo T_2-weighted MRI and (D) fluorescence image of tumor sites (insets) in tumor-bearing mice 1 hour after the intravenous injection of DOX-MVs and RGD–MVs–DOX, with (+) and without (−) application of a magnetic field. (E) Quantitative analysis of DOX fluorescence intensity in the corresponding tumor sites in (D). Reproduced with permission.[26] Copyright 2018, American Chemical Society

MNPs.[31] These biomimetic systems work by homotypic targeting and self-recognition, which results in internalization of the CCCM-coated theranostics by the cancer cells from which the membrane originated. However, in the clinic, the membrane coating would need to come from a patient's own cells, which poses challenges. It should also be noted that it can be difficult to extract the cell membrane with high purity.[32]

Targeted delivery systems also can be engineered based on materials sensitive to various stimuli, including endogenous stimuli (e.g., pH and enzymes), exogenous stimuli (e.g., US or magnetic) and combinations thereof.[33] For example, our group have prepared magnetic nanofibers for oral coadministration of SPIONs and the chemotherapeutic agent carmofur, using a pH-responsive polymer.[34] These fibers can protect the SPIONs in the acidic gastric conditions and release them at neutral pHs similar to those in the small intestine and colon. This could ultimately permit targeted and MRI-guided antitumor therapy. Further study showed that carmofur release could be quantified using T_2 MR relaxometry.[33] Xu and coworkers fabricated magnetically targeted liposomes carrying SPIONs, quantum dots, and cilengitide for active-targeted treatment of C6 glioma cells.[35] In vivo studies displayed enhanced drug delivery at the tumor, and accurate resection of the tumor site could be achieved with the aid of dual MRI-near infrared fluorescence (NIRF) imaging. In another study, polypeptide nanoparticles loaded with the anticancer agent cisplatin and SPIONs were developed for stimuli-responsive MRI-guided theranostics.[36] This system gave release of cisplatin and $Fe^{2+/3+}$ in response to the acidic tumor microenvironment, and an in vivo study

displayed selective accumulation in the tumor site by T_2-weighted MRI.

3.2 | T_1-MRI

Most of the theranostics discussed so far employ MNPs as negative CAs for T_2-weighted MRI. In some cases, however, negative-contrast MRI does not allow the CA signal to be differentiated from artifacts caused by pathological situations such as internal bleeding or calcification, or the boundaries between air and tissue.[37,38] To overcome these issues, a number of T_1-weighted MRI-guided theranostics have been developed.[39–41] Liu and colleagues fabricated poly(lactic acid)-based particles carrying gadolinium (Gd) ions chelated by DTPA groups and the chemotherapeutic agent sorafenib, seeking to target tumors overexpressing vascular endothelial growth factor receptor.[40] The contrast ability of Liu's nanomaterials was markedly improved compared to Magnevist®, a commercially available T_1 CA. In vivo studies revealed antitumor effects significantly better than those observed with free sorafenib. In another study, Ling developed a Gd-based nanoparticle–organic hybrid scaffold in which two chemotherapeutic agents, DOX and 5-fluorouracil (5-FU), were loaded.[41] High cytotoxicity to HeLa cells was observed as a result of synergistic pH-responsive release of DOX and 5-FU. Cellular uptake could be imaged using fluorescence and T_1-weighted MRI imaging.

To avoid the potential nephrotoxicity of Gd-based CAs, ultrasmall SPIONs have been explored as positive CAs.[42,43] The high surface area of these materials can facilitate the

interaction of paramagnetic $Fe^{2+/3+}$ centers with water protons, thus enhancing relaxation. It is reported that a particle size of approximately 5 nm is optimal to offer a high r_1 and a small r_2/r_1 ratio.[44] For example, Mosafer and coworkers developed PLGA-based nanoparticles encapsulating SPIONS and DOX and functionalized these with the AS1411 aptamer (APt), which actively targets nucleolin.[45] Greater tumor accumulation of APt-PLGA nanoparticles was observed in T_1 MRI, and effective anticancer properties were seen in mice models. Multifunctional theranostics have also been developed via integrating multiple imaging modalities such as dual T_1- and T_2-weighted MRI,[46] or MRI combined with computerized tomography (CT) and NIRF imaging.[47] Another approach to avoid Gd-related nephrotoxicity is to utilize manganese (Mn)-based formulations. For example, Shi et al. reported 2D MnO_2 nanosheets carrying a therapeutic siRNA with high loading efficiency and evaluated antitumor efficacy in a mice model.[48] The nanosheets displayed tumor microenvironment (TME)-triggered release of siRNA and permitted effective inhibition of tumor growth in vivo. This could be imaged by T_1-weighted MRI.

3.3 | Chemical exchange saturation transfer (CEST) MRI

The MRI signals generated by metal-based CAs can be affected by many conditions in vivo. To overcome these problems, the label-free strategy of CEST MRI has been developed. This is a combination of magnetic resonance spectroscopy (MRS) and MRI. MRS is a diagnostic technique that enables noninvasive identification and quantification of exogenous or endogenous chemicals, such as neurotransmitters, from localized portions of living tissue.[49] Without any magnetic label, chemical compounds (e.g., small molecule drugs) containing exchangeable protons with a resonance frequency different from water protons are selectively saturated using a specific MR frequency in CEST MRI. The magnetization of saturated protons is dephased into a plane vertical to longitudinal magnetization.[50,51] Exchange between water protons and saturated solute protons occurs (at exchange rates k_{sw} and k_{ws}; Figure 3A) and subsequently causes a transfer in saturation to water protons, which is controlled by scalar or dipolar spin–spin couplings (chemical exchange). As a result of this, the water proton signal in the ^1H NMR spectrum decreases slightly (Figure 3B). Since the water proton pools are much larger than the solute proton pool, the exchanged protons in the solute can be further saturated and exchanged again. When the protons have a sufficiently rapid exchange speed, and the saturation time (t_{sat}) is long enough, the unsaturated protons in the water pool contin-
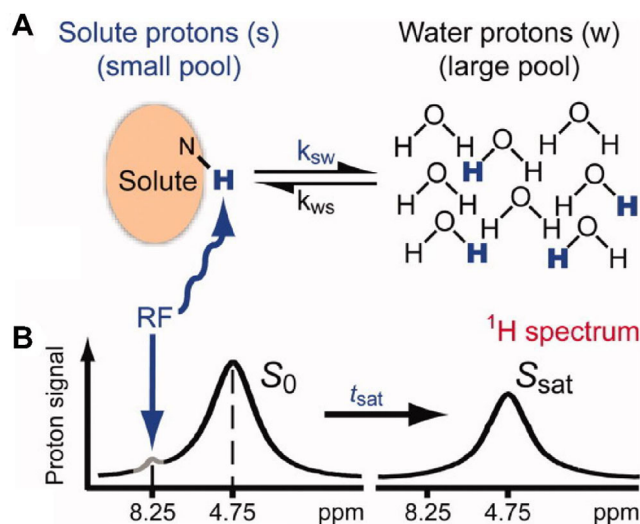

FIGURE 3 Illustration of CEST principles and the measurement approach. (A, B) Solute protons (blue) are saturated at their specific resonance frequency in the proton spectrum (here 8.25 ppm for amide protons). This saturation is transferred to water (4.75 ppm) at exchange rate k_{sw} and nonsaturated protons (black) are returned to the solute. After a period, this effect becomes visible in the ^1H NMR spectrum, as the water proton signals decrease from S_0 (B, left) to S_{sat} (B, right). Reproduced with permission.[52] Copyright 2011, Wiley VCH Verlag GmbH

uously take the place of the saturated solute protons. Thus, an elongated MR frequency can promote this saturation effect and leads to an enhancement of attenuation in the water signal, enabling solutes to be indirectly imaged with high sensitivity.[52]

CEST has a number of advantageous features. By exploiting an R_F presaturation pulse, the image contrast can be turned "on" and "off." As a result, CEST can be used for in vivo imaging of drug delivery,[53] or to monitor physiological parameters such as pH[54] and metabolite levels,[55,56] with good spatial resolution, excellent specificity and high sensitivity. A variety of CEST imaging acquisition approaches have been reported to enhance diagnosis and monitoring of ailments and metabolic disorders including cancerous tumors[56] and cartilage degeneration.[57]

Liu et al. found that the antineurodegeneration agent citicoline (cytidine-5′-diphosphocholine) is a promising CEST agent with high specificity.[53] Citicoline displayed excellent neuroprotective effects in a preclinical study, but clinical results on large populations were disappointing because ineffective delivery to the injured brain area compromised therapeutic outcomes. However, when concentrated in a liposome conjugated with active targeting ligands, citicoline could be effectively targeted and generate sufficient CEST MRI signal for imaging to be achieved.[58] In other work, the chemotherapy drug pemetrexed was conjugated with peptides and loaded into an injectable

hydrogel, and the resultant formulation found to permit noninvasive CEST MRI monitoring of drug delivery in a mouse glioma model.[49] A more detailed review on CEST MRI can be found in Ref. ([59]).

4 | THERANOSTICS FOR MRI-GUIDED THERMAL THERAPY

Thermal therapies for cancer treatment have gained increasing traction in recent decades as our understanding of the mechanisms behind heat-induced cell killing has improved, and advancements in technology have permitted controlled and localized heating. Thermal therapy is often preferred over chemotherapy because it can be localized and applied repeatedly in a minimally invasive fashion. A variety of techniques are now available for controlled and targeted heating, including lasers, high-intensity-focused US, radiofrequency currents or magnetic hyperthermia induced by MNPs.

MRI-guided thermal therapy is noninvasive and capable of target identification, real-time monitoring of treatment and closed-loop feedback. The latter can be used to further adjust the energy deposition pattern based on MRI. However, the application of high-energy stimuli to cause heating can lead to severe damage of the skin or healthy tissues surrounding the treatment areas. In some cases, the energy source is unable to yield the necessary extent of ablation (e.g., for large volume tumor masses or deep lesions). Signal intensity for imaging can also be a concern, with small lesions often being difficult to image owing to low MRI contrast. Hence, theranostics with high hyperthermia efficiency and powerful contrast potency are required to address these issues. Controlling thermal therapy at the tissue and cellular levels can be realized using targeting strategies, usually by exploiting nanoscale systems. Here we will give an overview of the MRI-guided systems that have been explored for different types of thermal therapy.

4.1 | MRI-guided magnetic hyperthermia therapy

Magnetic hyperthermia therapy (MHT) is a process whereby iron-based nanoparticles, such as SPIONs, generate heat under an alternating magnetic field arising from the size-dependent superparamagnetic properties of SPIONs. This can be exploited in cancer therapy because tumor cells are more susceptible to heat damage (and indeed other therapeutic interventions) than normal cells when the temperature ranges from 42°C to 45°C. SPIONs have been used in thermotherapy for a range of cancers,

including brain,[60] breast,[61] lung,[62] and liver cancers.[63] Since SPIONs are also excellent T_2 MRI CAs, they have been extensively studied as theranostics for MRI-guided MHT.

In favorable cases, SPIONs can be injected directly into the target tumor and are largely retained in it during repeated treatments. However, MHT suffers from problems with insufficient and uneven heating. When the tumor becomes smaller, the local concentration of SPIONs required to generate adequate thermal energy for hyperthermia dramatically increases based on a model of heat transfer in tissues.[64] Thus, a number of active targeting agents have been developed to enhance the efficacy of hyperthermia induction, as well as produce high quality MRI images to monitor the MHT outcome. In one study, Soleymani fabricated folate-targeted iron oxide nanoparticles (FA@Fe$_3$O$_4$ NPs) for simultaneous MRI imaging and MHT.[65] The active-targeted nanoparticles could selectively accumulate in the tumor site, as monitored by T_2-weighted MRI, and thereby enhance MHT efficacy.

In addition to SPIONs, other metal hybrid inorganic nanoclusters have also been developed as theranostics for MRI-guided MHT. For example, a Mn–Zn ferrite magnetic system was synthesized and conjugated with a fluorescent dye and peptide ligands to serve as a RGD receptor-tailed, dual-modal (MRI/fluorescence) agent for MHT.[66] However, it still remained impossible to provide adequate heating to ablate tumors. This arose due to low particle concentrations in the tumor site, despite the enhanced targeting effect of RGD. In other work, Kwon utilized a viral capsid particle to prepare inorganic nanocluster hybrids consisting of superparamagnetic gold nanoparticles (SPAuNC, Figure 4A) grafted with peptide ligands targeting the epidermal growth factor receptor (EGFR) ligands overexpressed on tumor cells.[67] In vivo studies revealed that this theranostic could actively target tumor cells and enhance T_2-weighted MRI and MHT (Figure 4B–D).

4.2 | MRI-guided US thermal therapy

US is a technique used clinically for both imaging and therapy. It is characterized by its ability to penetrate deep lesions. Recently, temperature-sensitive MRI has been used to guide US surgery for selective tumor ablation based on calculated results of thermal dose from multislice images.[68,69] MRI-guided US surgery successfully removed tumors within a planned area in the prostates of both canines and humans using a directional transurethral US applicator.[69]

However, high-energy acoustic waves are required to heat effectively in US, which might lead to damage to nearby healthy tissues. As a result, efforts have been
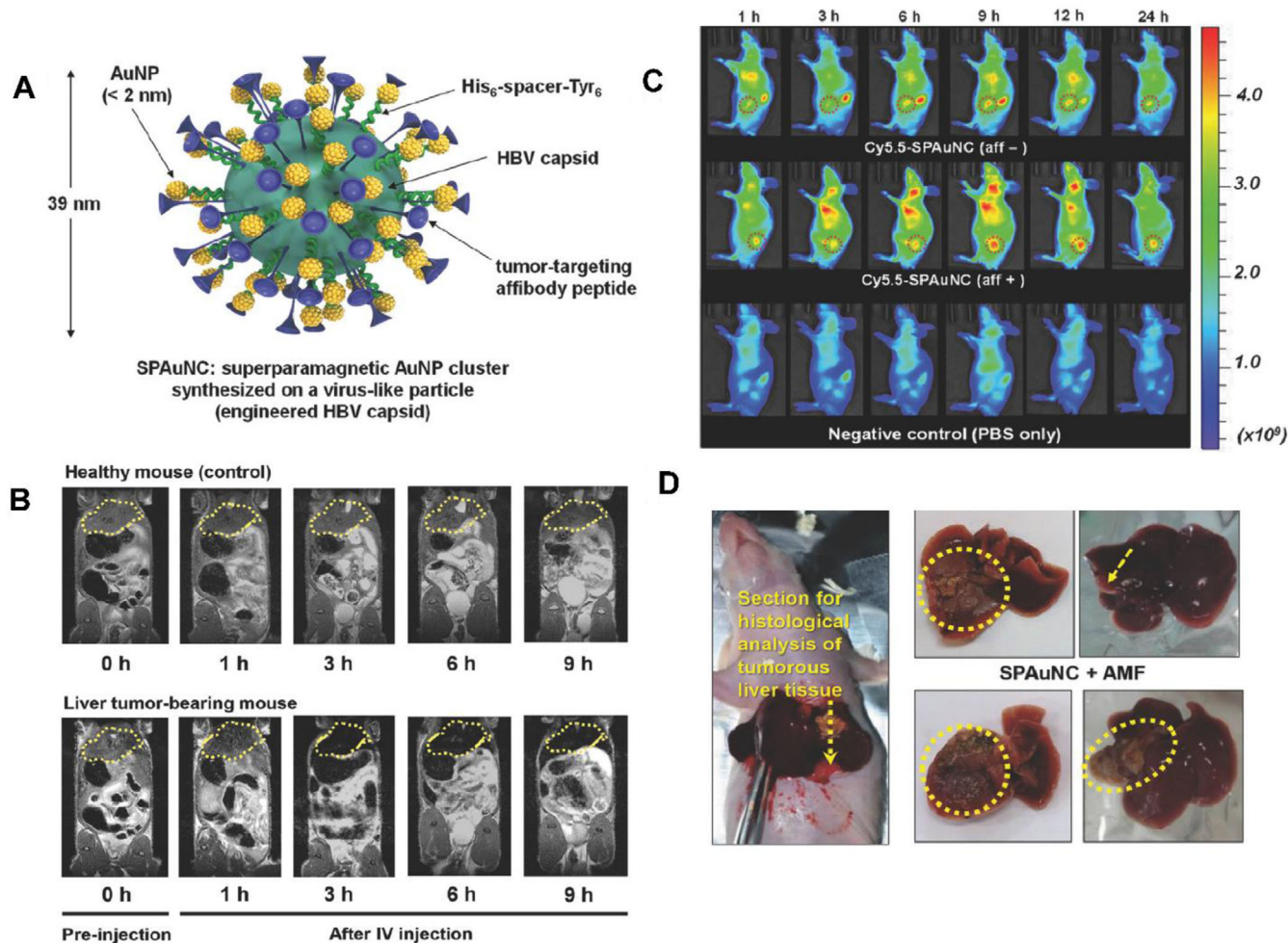
FIGURE 4 (A) Schematic image of an SPAuNC. (B) Time-course T_2-weighted MR images of mice bearing a liver tumor and healthy mice obtained using SPAuNC functionalized with a peptide ligand (aff +). (C) NIRF images of mice bearing a subcutaneous tumor at various predetermined time points after the intravenous injection of Cy5.5-SPAuNC with (aff +) or without peptide functionalization (aff −). (D) Photographs of mice bearing a subcutaneous tumor that were treated (right, top) or not treated (right, bottom) by functionalized SPAuNC (aff +). Reproduced with permission.[67] Copyright 2017, Wiley VCH Verlag GmbH

undertaken to prepare thermosensitive agents to improve the heating efficiency. For instance, a thermosensitive magnetic-guided active targeting liposome incorporating fullerene (C_{60}), SPIONs and docetaxel (DTX) has been developed.[70] This was found able to act as a radiofrequency thermal therapy agent, which can trigger the release of DTX as observed in T_2-weighted MRI and eradicate the cancer cells by heat energy generated from radiofrequency irradiation. A more recent study reported a Gd-labeled thermoresponsive liposome that can be concentrated in a tumor.[71] A subsequent burst of focused US (3 minutes) caused it to release a DOX payload, thus allowing highly targeted treatment. The accumulation of liposomes at the tumor site also caused a reduction of the T_1 relaxation time.

To improve therapeutic outcomes, MRgFUS has been widely studied as a route to use MRI to guide US-mediated thermoablation.[62] In the clinic, the US energy source must be precisely controlled, which can be achieved in MRg-FUS by using MRI to provide details of changes at and around the treatment area. For example, gradient echo MR imaging can be used to record the temperature in real time during MRgFUS treatment. This is achieved by monitoring the relaxation time and exploiting the temperature sensitivity of the proton resonance frequency. Wang et al. proposed a SPION nanosystem that actively targets EGFR, since the latter was overexpressed in a number of epithelial tumors.[62] This active targeting system led to significant enhancement of MRI sensitivity in rat models. When applying MRgFUS, the SPION-based theranostics could lead to effective ablation of a tumor at a relatively low energy level. Recently, a novel focused US hyperthermia approach using ultrashort (~30 seconds) thermal exposures (~41°C to 45°C) was reported to trigger the release of DOX from a thermoresponsive liposomal system
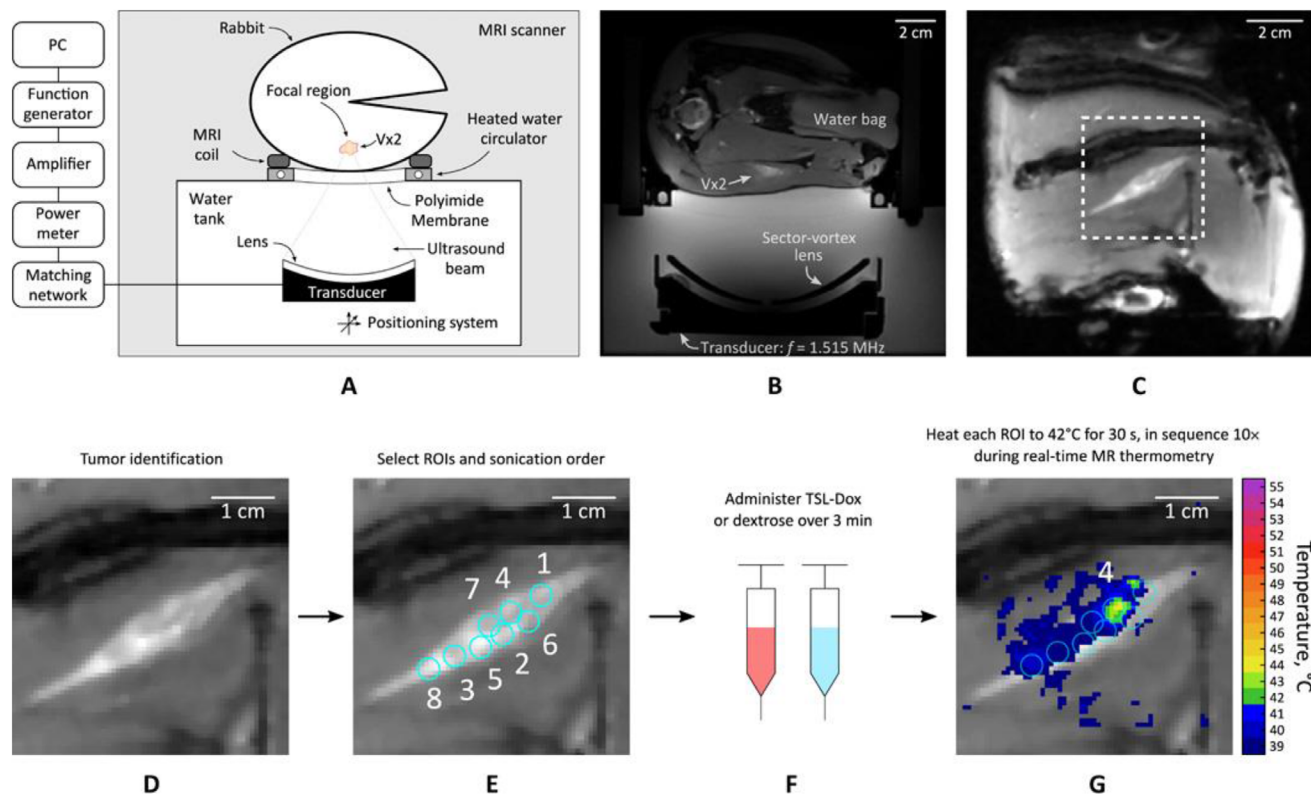
FIGURE 5 (A) Schematic illustration of the MRgFUS experimental setup. (B) Axial contrast-enhanced T_1-weighted MR image of a rabbit bearing a tumor, recorded with the MRI-compatible FUS setup. (C) Coronal MR image. The experimental paradigm involves (D) tumor identification, followed by (E) the selection of regions of interest (ROIs) within the tumor to be specifically heated. Treatment then proceeds via (F) the administration of thermoresponsive liposomes (TSL-Dox) or dextrose (negative control), and (G) real-time MRgFUS thermometry of the tumor. Reproduced with permission.[72] Copyright 2020, American Association for the Advancement of Science

(Figure 5).[72] Real-time temperature feedback was obtained using magnetic resonance thermometry during a hyperthermia treatment, and in vivo experiments showed that tumor growth was significantly inhibited.

4.3 | MRI-guided photothermal therapy

Photothermal therapy (PTT) is another minimally invasive therapeutic approach that has been combined with MRI. PTT works to ablate cancer cells by generating heat energy from electromagnetic radiation. This is generally achieved by using a photoabsorbing agent to absorb near-infrared (NIR) light from a laser and convert this to heat. PTT can be designed to specifically target tumors with spatial and temporal precision.[73] Factors affecting the therapeutic efficacy of PTT include the incident excitation energy (e.g., the light intensity) and the dosage and photothermal conversion efficiency (PTCE) of the PTT agents. A number of PTT agents based on inorganic, organic, carbon, or semiconductor materials have been explored, seeking to prepare systems with (i) high PTCE, typically seeking strong absorption of NIR light; (ii) excellent targeting capability; and (iii) low toxicity and high biocompatibility.[74]

Since MRI CAs (e.g., Gd-based agents and SPIONs) tend to have low PTCE, they must be combined with photoactive materials for MRI-guided PTT. One targeted platform for theranostic MRI and fluorescence imaging and PTT was prepared via conjugation of hyaluronic acid and CuInS$_2$-ZnS quantum dots on the surface of a magnetic Prussian blue.[74] In a murine HeLa tumor model, this system exhibited effective uptake in the tumor site using both magnetic and CD44 receptor active targeting. Uptake could be monitored by MRI and NIR fluorescence, and the formulation led to significant temperature rises (up to around 49°C) and thus had excellent in vivo PTT efficacy.[75] More recently, a metal-free nanosystem was designed for MRI-guided tumor-targeted PTT, as shown in Figure 6.[76] This consisted of a glycol chitosan–polypyrrole (GC–PP) scaffold modified with a nitroxide radical (TEMPO) and folic acid (FA). The GC–PP@TEMPO–FA nanoparticles demonstrated a high loading of nitroxide radicals with excellent stability and prolonged circulation time, and the paramagnetic property of the TEMPO protons can reduce water proton longitudinal relaxation times, providing T_1 contrast ability. In vivo studies using a tumor-bearing model displayed enhancement of T_1-weighted MRI signals over 17 hours and generated excellent PTT performance.
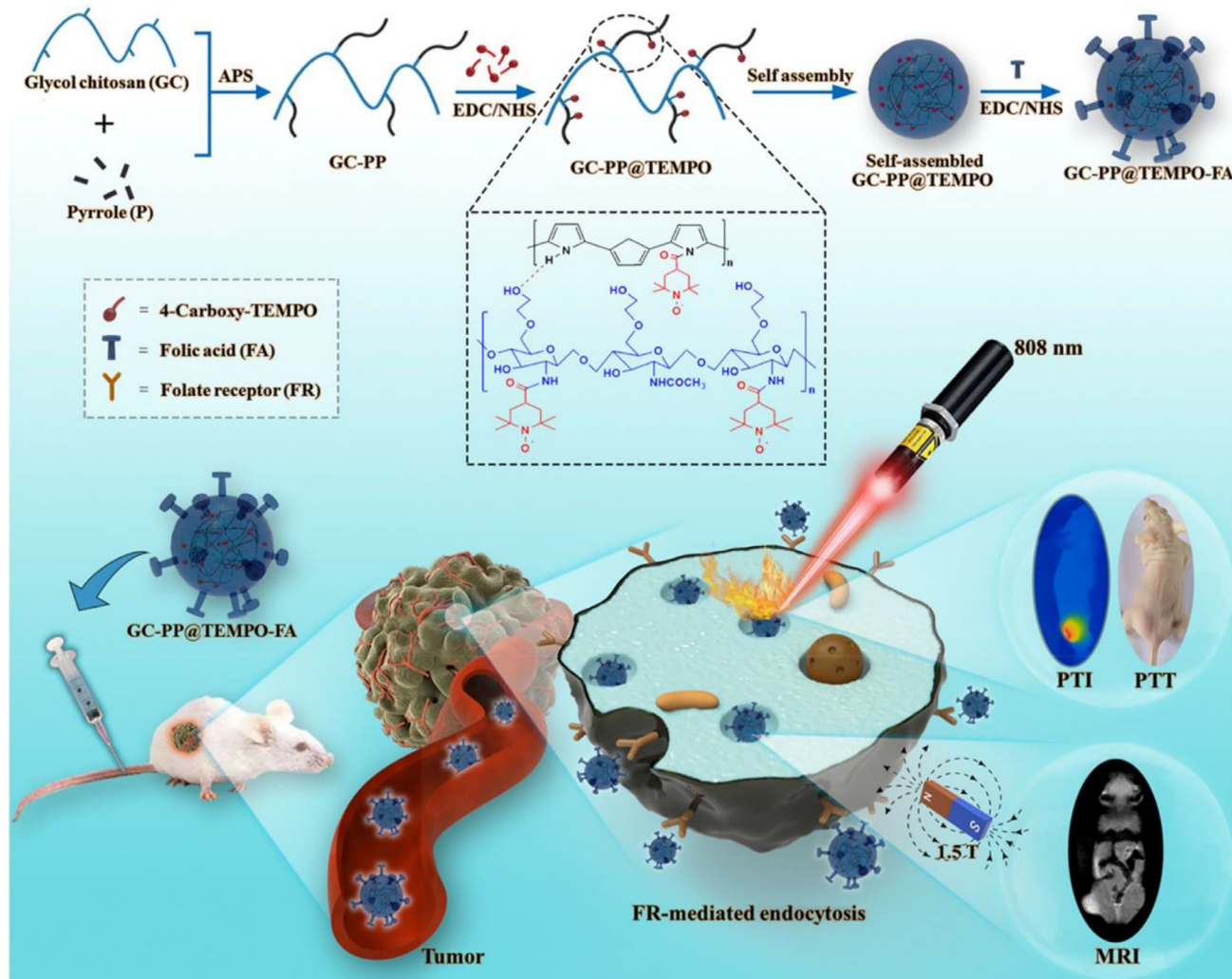
FIGURE 6 Schematic diagram of the synthesis of self-assembled and active targeted nanoparticles providing in vivo MRI-guided PTT. Reproduced with permission.[76] Copyright 2021, American Chemical Society

Magnetic targeting has been used to deliver PTT agents and improve photostability, biodistribution, and pharmacokinetics. For example, indocyanine green (ICG) is a clinically approved photothermal agent for fluorescent-guided surgery but suffers from poor photostability and low bioavailability. Incorporating ICG into nanovehicles increases the circulation time and enhances targeted delivery into tumors.[77] In one study, a magnetic nanocluster consisting of a Fe_3O_4 core and a polydopamine shell grafted with polyethylene glycol and ICG was fabricated for combined MRI and PTT.[78] The formulation could be magnetically targeted to accumulate in HepG2 liver tumors in a mouse model, and improved the efficacy of PTT because of the presence of two NIR absorbers, (polydopamine and ICG). The therapeutic process could be monitored by T_2-weighted MRI and an infrared thermal camera. More recently, polydopamine-coated mesoporous silica particles loaded with manganese ions were proven to be potent T_1 MRI CAs and photosensitizing

agents with excellent PTCE in an in vivo mice model.[79] Beik and coworker established a computational model to simulate the heat transfer process in the tumor during PTT, based on MRI data and nanoparticle distribution in vivo. This allowed accurate predictions of the in vivo performance.[80]

Recent studies have provided a variety of approaches to enhance MRI-guided PTT efficacy, including employing absorbance in the NIR-II window (900–1700 nm) to reduce noise arising from autofluorescence and photon scattering, and enhance the penetration depth.[80,81] Other work sought to combine MRI with other imaging modalities such as photoacoustic imaging (PAI) or US,[82,83] or use subcellular targeting strategies to deliver a payload selectively to the nucleus.[84] 1D-ferrous phosphide nanorods were developed by Liu as a multimodal theranostic for T_2 MRI/PAI and enhanced PTT.[85] This formulation allowed PTT (with high PTCE in the NIR II window) to be combined with chemodynamic therapy, providing a promising

platform for targeted, controllable, antitumor treatment with simultaneous MRI/PAI.

PTT can result in local tissue temperatures over 50°C, which can be harmful to healthy surrounding tissues. To avoid this issue, mild photothermal treatment (MPTT) has been devised, seeking to ensure a maximum temperature of around 45°C. Such low temperatures do not usually result in effective PTT, because the cell damage induced by mild heating stress tends to be repaired by a cell's intrinsic thermo resistance system with the aid of heat shock proteins. Thus, strategies have been developed to permit effective PTT at lower temperatures.[86]

One such approach is to convert oxygen radicals induced by heat stress to highly toxic reactive oxygen species (ROS) such as •OH.[87] Moderate hyperthermia can increase the oxygen concentration in cells by reducing oxygen consumption via alternation of cell metabolism pathways and inhibition of cell respiration.[88] In one study, Qiu et al. fabricated magnetic nanoparticle–iridium (III) complexes that actively targeted mitochondria and could efficiently kill tumor cells upon NIR laser irradiation.[89] The nanoparticles were seen to accumulate in the tumor site of mouse models, using T_2-weighted MRI. Cell apoptosis was induced by generation of •OH at a local temperature of 42°C. MPTT has also been used to sensitize cancer cells to immunotherapy and chemotherapy.[90,91] In another study, Huang exploited MPTT as a complementary therapy to enhance the therapeutic outcome of the chemotherapeutic drug SN38. In vivo studies showed that the integration of chemotherapy and MPTT gave better performance in inhibition of bone tumor growth and alleviation of osteolytic damage at temperatures around 43°C than chemotherapy or MPTT alone.[92]

5 | THERANOSTICS FOR MRI-GUIDED COMBINATION THERAPIES

Combination therapies are desirable in a number of disease settings to avoid drug resistance, lower the required dosage, and reduce adverse effects. In this section, MRI-trackable theranostics for multimodal therapy will be outlined.

5.1 | Photodynamic (PDT)— photothermal (PTT)—chemotherapy

One major drawback of PTT is the uneven distribution of heat and restricted tissue penetration, which can lead to unsuccessful tumor ablation and a high risk of cancer recurrence.[93] The combination of PTT with other therapeutic approaches such as photodynamic therapy (PDT)[94–96] and chemotherapy[97,98] has been found helpful to overcome this challenge, particularly for complex, large, and heterogeneous tumors. For instance, an iron-based nanoparticle with T_1/T_2 MRI contrast ability has been developed as a theranostic platform to deliver DOX and conduct PTT.[99] In vivo studies in tumor-bearing mice showed that the system could be accumulated in a tumor as a result of the enhanced permeation and retention (EPR) effect, as well as enhancing both T_1 and T_2-weighted MRI. Excellent tumor-killing effects were observed as a result of the synergy between chemotherapy and PTT.

PDT is a minimally invasive and targeted therapy, which works by local generation of highly active ROS. These are formed by energy transferred from light activation of photosensitizers.[100,101] PDT agents are nontoxic in the dark, which makes the therapeutic process highly controllable. Recently, MRI-trackable agents to combine PDT-PTT therapy have attracted increasing attention. For example, a multifunctional smart nanoplatform was developed for combined PTT–PDT therapy, which could be imaged by T_1-weighted MRI.[102] The formulation was composed of a tumor-microenvironment sensitive carbon nanotube scaffold loaded with a photosensitizer (Ce6), and MnO_2. In the low pH of the TME, Ce6 was rapidly released for PDT, and Mn^{2+} was freed into solution for T_1 MRI. The authors showed that MnO_2 helped to catalytically decompose the excess H_2O_2 present in the tumor into O_2, which can further promote ROS production and enhance PDT efficacy. Guo and coworkers prepared a MnO_2 based nanoenzyme loaded with polypyrrole and evaluated its therapeutic effect as an MRI-guided PTT–PDT agent in tumor-bearing mice.[103] The results showed that the nanoenzyme gave enhanced T_1 contrast and outstanding tumor ablation performance. Another PDT–PTT–chemotherapy platform based on black phosphorus nanosheets (BPN) was reported by Wu et al.[104] When decorated with MnO_2 nanosheets, the BPN system exhibited enhanced phototherapeutic potency. The time-dependent accumulation of the formulation in the tumor site was clearly shown in T_1-weighted MRI images. In other work, Lin et al. reported a Prussian blue nanoparticle grafted with polydopamine and Ce6 as a multifunctional theranostic for combined PTT and PDT.[105] Both In vivo and in vitro studies confirmed inhibition of tumor growth and moderate enhancement in T_2-weighted MRI.

Feng and coworkers fabricated a combined PTT–PDT–chemotherapy theranostic consisting of magnetic mesoporous CuS particles loaded with DOX.[106] When exposed to NIR irradiation DOX release could be triggered, and PTT–PDT combined therapy was achieved via localized surface plasmon resonance and increasing ROS levels caused by the leakage of copper ions. T_2 MRI can be used to monitor the resultant therapeutic effects. Using multiple targeting approaches can further enhance the efficacy of chemotherapy–PTT, while combining this with MRI capabilities enables accurate and real-time imaging of the
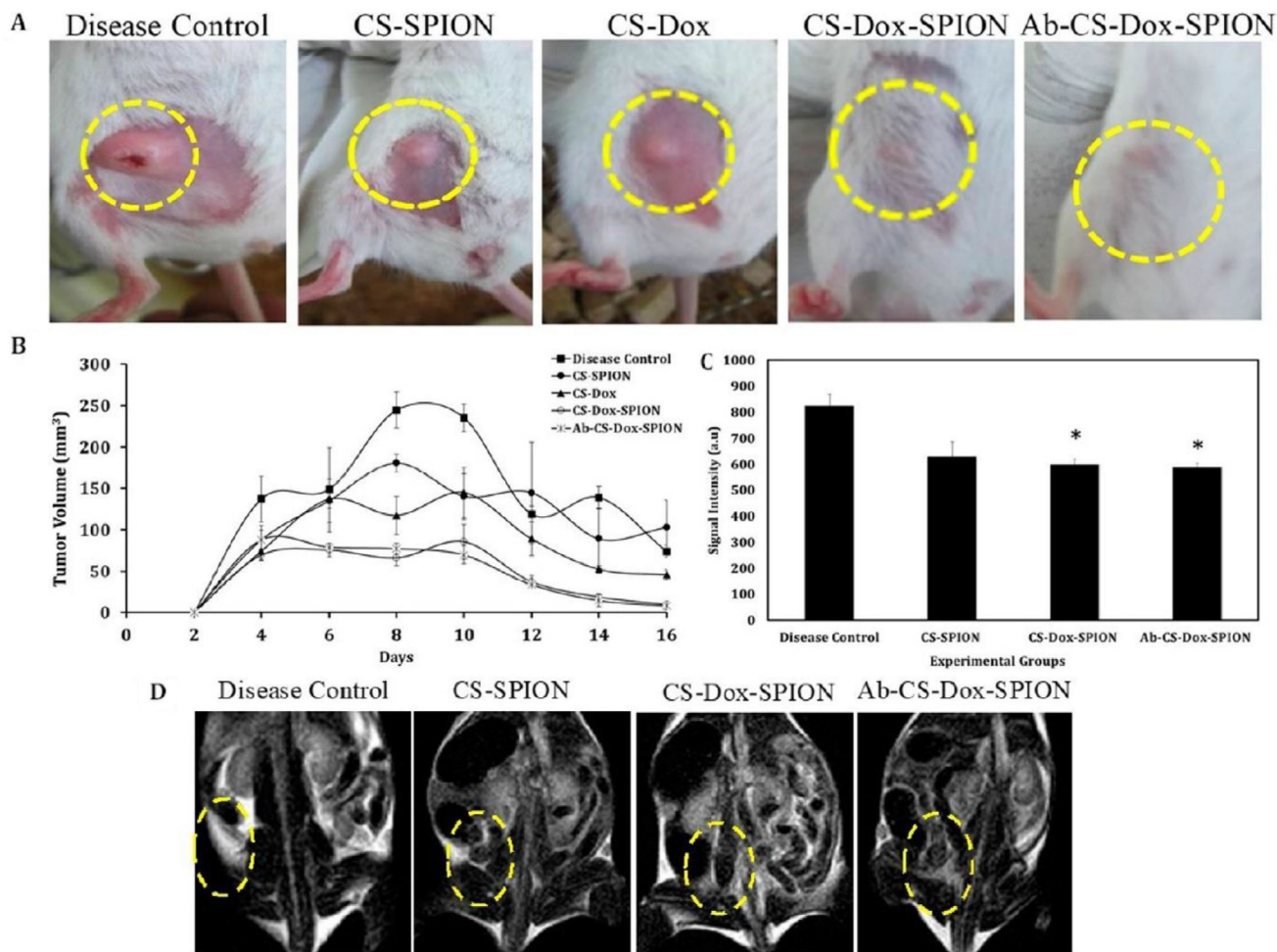
FIGURE 7 (A) Photographs of TNBC tumor bearing Balb/c mice treated with chitosan (CS)–SPION, CS–Dox, CS–Dox–SPION, and Ab–CS–Dox–SPION formulations. (B) Tumor volumes over 16 days (error bars indicate the standard error of mean, $n = 5$). (C) T_2 signal intensity changes at the tumor site ($P < 0.05$, *denotes significance with respect to disease control) and (D) T_2-weighted MR images. Dotted circles denote the region of interest. Reproduced with permission.[110] Copyright 2018, American Chemical Society

therapeutic effect. A variety of active targeting platforms have been developed to this end, such as: folate-conjugated Ag-Fe$_3$O$_4$ particles carrying DOX[81]; EGFR-targeted erbitux-modified liposomes loaded with gold nanorods and DOX[98]; PLGA-coated Fe$_3$O$_4$ graphene oxide nanomaterials containing 5-fluoruracil (5-FU)[107]; and polymer hybrid MNPs carrying the photosensitizer IR820 and PTX.[97] All the systems have been shown to be potent in MRI-monitoring of PTT–chemotherapy treatments.

5.2 | Magnetic hyperthermia (MHT)—chemotherapy

As discussed above, MHT can be an effective treatment for cancer, enabling an elevation of local temperature to promote other treatment such as chemotherapy.[108] SPIONs can thus be used to make cancer cells vulnerable, and additionally have inherent MRI CA properties. A magnetic targeting thermoresponsive theranostic nanoplatform was

devised by Li and coworkers to combine MHT with magnetothermally-facilitated release of DOX.[109] In vivo T_2-weighted MRI experiments proved that, via magnetic targeting, the formulation was accumulated at the tumor with a prolonged retention time. This reduces DOX distribution to off-target tissues including the heart and kidneys, and promotes the cellular uptake of DOX. More recently, Manigandan et al. fabricated a $\alpha v \beta 3$-targeted chitosan micellar nanoplatform carrying DOX–SPION complexes (Ab–CS–Dox–SPION).[110] This material integrated chemotherapy and MHT to treat mice bearing triple-negative breast cancer (TNBC) tumors. TNBC is the most lethal metastatic breast cancer, with average survival times of only 13–18 months.[111] Manigandan's system showed effective targeting, with greater accumulation at the tumor site than nontargeted particles (as shown in T_2-weighted MRI), and MHT–chemotherapy significantly inhibited both primary tumor growth and metastasis (Figure 7A–D). In another study, magnetic nanocrystals

were developed by Liu et al., who synthesized RGD-conjugated Mn–Zn ferrite particles (MNCs) loaded with PTX in a lipid surface layer.[110] In a breast tumor-bearing mouse model, the RGD–MNCs–PTX nanoparticles displayed high negative MRI contrast and outstanding magnetism-induced heat generation. With the aid of in vivo MRI, the formulation was seen to be effectively targeted to tumor neovascular epithelial cells. Upon reaching the target site, the local temperature increase caused by MHT subsequently led to a burst release of PTX.

6 | CONCLUSIONS

Nanotechnology makes it possible to integrate active targeting with MRI and other imaging/therapy modalities and thereby improve the efficacy of personalized medicine. Recent developments of multifunctional theranostics are discussed in this review, with a focus on formulations comprised of targeting agents, therapeutic molecules and MRI CAs. We discuss these in the context of MRI-traceable targeted and controllable drug delivery, using MRI to guide thermal treatments such as PTT and MHT, and MRI-guided synergistic therapy, as well as considering theranostics with multimodal imaging capabilities. Many of these systems have shown promise in in vivo experiments, and some have begun translation to the clinic. Future tactics to improve therapeutic outcomes are likely to involve combinatorial therapies, especially in the case of aggressive heterogeneous and multidrug resistant tumors. Nanoparticles are ideally suited to this goal. However, complex synthesis protocols are often required to generate nanoparticulate theranostic formulations, which poses challenges in terms of reproducibility and translation from bench to clinic. Few studies have focused on this issue, and in the authors' view future research should focus on finding solutions to produce nanoplatforms via facile routes suitable for clinical translation.

CONFLICT OF INTEREST
The authors declare that there is no conflict of interest.

ORCID
Gareth R. Williams https://orcid.org/0000-0002-3066-2860

REFERENCES

1. B. Du, M. Yu, J. Zheng, *Nat. Rev. Mater.* **2018**, *3*, 358.
2. M.-J. Mitchell, M.-M. Billingsley, R.-M. Haley, M.-E. Wechsler, N.-A. Peppas, R. Langer, *Nat. Rev. Drug Discov.* **2021**, *20*, 101.
3. H. Wang, P. Agarwal, Y. Xiao, H. Peng, S. Zhao, X. Liu, S. Zhou, J. Li, Z. Liu, X. He, *ACS Cent. Sci.* **2017**, *3*, 875.
4. G. Pillai, *SOJ Pharm. Pharm. Sci.* **2014**, *1*, 13.
5. E. Acosta, *Curr. Opin. Colloid In.* **2009**, *14*, 3.
6. D. Arora, S. Jaglan, *Trends Food Sci. Tech.* **2016**, *54*, 114.
7. S.-S. Kelkar, T.-M. Reineke, *Bioconjug. Chem.* **2011**, *22*, 1879.
8. J.-H. Turner, *Br. J. Radiol.* **2018**, *91*, 20170893.
9. T. Anani, S. Rahmati, N. Sultana, A.-E. David, *Theranostics* **2021**, *11*, 579.
10. S. Karahisar, T.-H. Yildizhan, N.-P. Barkan, F.-D.-Ö. Demiralp, B. Uslu, S.-A. Ozkan, *Design of Nanostructures for Theranostics Applications*, William Andrew Publishing, United States, **2018**.
11. J. Xie, J. Jiang, P. Davoodi, M.-P. Srinivasan, C.-H. Wang, *Chem. Eng. Sci.* **2015**, *125*, 32.
12. V.-S. Khoo, D.-P. Dearnaley, D.-J. Finnigan, A. Padhani, S.-F. Tanner, M.-O. Leach, *Radiother. Oncol.* **1997**, *42*, 1.
13. E. Debroye, T.-N. Parac-Vogt, *Chem. Soc. Rev.* **2014**, *43*, 8178.
14. C. Verry, S. Dufort, B. Lemasson, S. Grand, J. Pietras, I. Troprès, Y. Crémillieux, F. Lux, S. Mériaux, B. Larrat, J. Balosso, G.-L. Duc, E.-L. Barbier, O. Tillement, *Sci. Adv.* **2020**, *15*, eaay5279.
15. E. Boros, E.-M. Gale, P. Caravan, *Dalton Trans.* **2015**, *44*, 4804.
16. M.-T. Vlaardingerbroek, J. A. Boer, *Magnetic resonance imaging: theory and practice.* Springer Science & Business Media, United States, **2013**.
17. D. Hao, T. Ai, F. Goerner, X. Hu, V.-M. Runge, M. Tweedle, *J. Magn. Reason. Imaging* **2012**, *36*, 1060.
18. P. Caravan, *Chem. Soc. Rev.* **2006**. *35*, 512.
19. J. Estelrich, M.-J. Sánchez-Martín, M.-A. Busquets, *Int. J. Nanomedicine* **2015**, *10*, 1727.
20. L.-L. Israel, A. Galstyan, E. Holler, J.-Y. Ljubimov, *J. Control Release* **2020**, *320*, 45.
21. L.-P. Ganipineni, B. Ucakar, N. Joudiou, J. Bianco, P. Danhier, M. Zhao, C. Bastiancich, B. Gallez, F. Danhier, V. Préat, *Int. J. Nanomedicine* **2018**, *13*, 4509
22. A. Abrahao, Y. Meng, M. Llinas, Y. Huang, C. Hamani, T. Mainprize, I. Aubert, C. Heyn, S.-E. Black, K. Hynynen, N. Lipsman, L. Zinman, *Nat. Commun.* **2019**, *26*, 4373.
23. C.-H. Fan, Y.-H. Cheng, C.-Y. Ting, Y.-J. Ho, P.-H. Hsu, H.-L. Liu, C.-K. Yeh, *Theranostics* **2016**, *18*, 1542.
24. D. Liu, D.-T. Auguste, *J. Control Release* **2015**, *219*, 632.
25. W.-H. Chen, G.-F. Luo, Q. Lei, F.-Y Cao, J.-X. Fan, W.-X. Qiu, H.-Z Jia, S. Hong, F. Fang, X. Zeng, R.-X. Zhuo, X.-Z. Zhang, *Biomaterials* **2016**, *76*, 87.
26. K. Yang, Y. Liu, Y. Liu, Q. Zhang, C. Kong, C. Yi, Z. Zhou, Z. Wang, G. Zhang, Y. Zhang, N.-M. Khashab, X. Chen, Z. Nie, *J. Am. Chem. Soc.* **2018**. *140*, 4666.
27. J.-M. Shen, X.-X. Li, L.-L. Fan, X. Zhou, J.-M. Han, M.-K. Jia, L.-F. Wu, X.-X. Zhang, J. Chen, *Int. J. Nanomedicine* **2017**, *12*, 1183.
28. P.-L. Rodriguez, T. Harada, D.-A. Christian, D.-A Pantano, R.-K. Tsai, D.-E. Discher, *Science* **2013**, *339*, 971.
29. C.-M. Hu, R. Fang, K.-C. Wang, B.-T. Luk, S. Thamphiwatana, D. Dehaini, P. Nguyen, P. Angsantikul, C. H. Wen, A.-V. Kroll, C. Carpenter, M. Ramesh, V. Qu, S.-H. Patel, J. Zhu, W. Shi,

F.-M. Hofman, T.-C. Chen, W. Gao, K. Zhang, S. Chien, L. Zhang, *Nature* **2015**, *526*, 118.

30. A. Parodi, N. Quattrocchi, A.-L. van de Ven, C. Chiappini, M. Evangelopoulos, J.-O. Martinez, B.-S. Brown, S.-Z. Khaled, I.-K. Yazdi, M.-V. Enzo, L. Isenhart, M. Ferrari, E. Tasciotti, *Nat. Nanotechnol.* **2013**, *8*, 61.

31. J.-Y. Zhu, D.-W. Zheng, M.-K. Zhang, W.-Y. Yu, W.-X. Qiu, J.-J. Hu, J. Feng, X.-Z. Zhang, *Nano Lett.* **2016**, *14*, 5895.

32. J.-C. Harris, M.-A. Scully, E.-S. Day, *Cancers* **2019**, *11*, 1836.

33. L. Li, W.-W. Yang, D.-G. Xu, *J. Drug Target* **2019**, *27*. 423.

34. Z. Zhang, C.-J.-R. Wells, A.-M. King, J.-C. Bear, G.-L. Davies, G.-R. Williams, *J. Mater. Chem. B* **2020**, *8*, 7264.

35. H.-L. Xu, J.-J. Yang, D.-L. ZhuGe, M.-T. Lin, Q.-Y. Zhu, B.-H. Jin, M.-Q. Tong, B.-X. Shen, J. Xiao, Y.-Z. Zhao, *Adv. Healthc. Mater.* **2018**, *7*, 1701130.

36. Z. Gao, T. He, P. Zhang, X. Li, *ACS Appl. Mater. Interfaces* **2020**, *12*, 20271.

37. S. Cakirer, E. Karaarslan, A. Arslan, *Curr. Probl. Diagn. Radiol.* **2003**, *32*, 194.

38. D.-W. Shattuck, S.-R. Sandor-Leahy, K.-A. Schaper, D.-A. Rottenberg, R.-M. Leahy, *NeuroImage* **2001**, *13*, 856.

39. Y. Cheng, X. Tan, J. Wang, Y. Wang, Y. Song, Q. You, Q. Sun, L. Liu, S. Wang, F. Tan, J. Li, N. Li, *J. Control Release* **2018**, *277*, 77.

40. Y. Liu, L. Feng, T. Liu, L. Zhang, Y. Yao, D. Yu, L. Wang, N. Zhang, *Nanoscale* **2014**, *6*, 3231.

41. D. Ling, H. Li, W. Xi, Z. Wang, A. Bednarkiewicz, S. T. Dibaba, L. Shi, L. Sun, *J. Mater. Chem. B* **2020**. *8*, 1316.

42. S. Caspani, R. Magalhães, J.-P. Araújo, C.-T. Sousa, *Materials (Basel)* **2020**, *5*, 2586.

43. C. Dua, J. Wang, X. Liu, H. Li, D. Geng, L. Yu, Y. Chen, J. Zhang, *Biomaterials* **2020**, *230*, 119581.

44. F. Hu, Q. Jia, Y. Li, M. Gao, *Nanotechnology* **2011**, *22*, 245604.

45. J. Mosafer, K. Abnous, M. Tafaghodi, A. Mokhtarzadeh, M. Ramezani, *Eur. J. Pharm. Biopharm.* **2017**, *113*, 60.

46. G. Wang, X. Zhang, Y. Liu, Z. Hu, X. Mei, K. Uvdal, *J. Mater. Chem. B* **2015**, *15*, 3072.

47. G. Wang, K. Qian, X. Mei, *Nanoscale* **2018**, *10*, 10467.

48. M. Shi, S. Wang, S. Zheng, P. Hou, L. Dong, M. He, C. Wu, X. Zhang, F. Zuo, K. Xu, J. Li, *Colloids Surf. B. Biointerfaces* **2020**, *185*, 10625.

49. C. Stagg, D.-L. Rothman, *Magnetic Resonance Spectroscopy: Tools for Neuroscience Research and Emerging Clinical Applications.* Academic Press, United States, **2013**.

50. S. Mori, M.-O. Johnson, J.-M. Berg, P.-C. M. van Zijl, *J. Am. Chem. Soc.* **1994**, *116*, 11982.

51. W.-S. Price, *NMR Studies of Translational Motion: Principles and Applications.* Cambridge University Press, United Kingdom, **2009**.

52. P.-C.-M. van Zij, N.-N. Yadav, *Magn. Reason. Med.* **2011**, *65*, 927.

53. H. Liu, A. Jablonska, Y. Li, S. Cao, D. Liu, H. Chen, P.-C. Van Zijl, J.-W M Bulte, M. Janowski, P. Walczak, G. Liu, *Theranostics* **2016**, *18*, 1588.

54. S. Aime, D. Delli Castelli, E. Terreno, *Angew. Chem. Int. Ed.* **2002**. *41*, 4334.

55. D.-L. Longo, A. Bartoli, L. Consolino, P. Bardini, F. Arena, M. Schwaiger, S. Aime. *Cancer Res.* **2016**, *76*, 6463.

56. A. Anemone, L. Consolino, L. Conti, P. Irrera, M.-Y. Hsu, D. Villano, W. Dastrù, P.-E. Porporato, F. Cavallo, D.-L. Longo, *Br. J. Cancer* **2021**, *124*, 207.

57. T.-M. Link, J. Neumann, X. Li, *J. Magn. Reason. Imaging* **2017**, *45*, 949.

58. L.-L. Lock, Y. Li, X. Mao, H. Chen, V. Staedtke, R. Bai, W. Ma, R. Lin, Yi Li, G. Liu, H. Cui, *ACS Nano* **2017**, *11*, 797.

59. Z. Han, G. Liu, *Biomed. Mater.* **2021**, *16*, 024103.

60. A. Jordan, R. Scholz, K. Maier-Hauff, F.-K.H. van Landeghem, N. Waldoefner, U. Teichgraeber, J. Pinkernelle, H. Bruhn, F. Neumann, B. Thiesen, A. von Deimling, R. Felix, *J. Neurooncol.* **2006**, *78*, 7.

61. I. Hilger, R. Hergt, W.-A. Kaisera, *J. Magn. Magn. Mater.* **2005**, *293*, 314.

62. Z. Wang, R. Qiao, N. Tang, Z. Lu, H. Wang, Z. Zhang, X. Xue, Z. Huang, S. Zhang, G. Zhang, Y. Li, *Biomaterials* **2017**, *127*, 25.

63. S. Yan, D. Zhang, N. Gu, J. Zheng, A. Ding, Z. Wang, B. Xing, M. Ma, Y. Zhang, *J. Nanosci. Nanotechnol.* **2005**, *5*, 1185.

64. B. Kozissnik, A.-C. Bohorquez, J. Dobson, C. Rinaldi, *Int. J. Hyperthermia.* **2013**, *29*, 706.

65. M. Soleymani, S. Khalighfard, S. Khodayari, H. Khodayari, M.-R. Kalhori, M.-R. Hadjighassem, Z. Shaterabadi, A.-M. Alizadeh, *Sci. Rep.* **2020**, *10*, 1695.

66. J. Xie, C. Yan, Y. Yan, L. Chen, L. Song, F. Zang, Y. An, G. Teng, N. Gu, Y. Zhang, *Nanoscale* **2016**, *8*, 16902.

67. K.-C. Kwon, E. Jo, Y.-W. Kwon, B. Lee, J.-H. Ryu, E.-J. Lee, K. Kim, J. Lee, *Adv. Mater.* **2017**, *29*, 38.

68. J.-D. Hazle, C.-J. Diederich, M. Kangasniemi, R.-E. Price, L.-E. Olsson, R.-J. Stafford, *J. Magn. Reason. Imaging* **2002**, *15*, 409.

69. K. Siddiqui, R. Chopra S. Vedula, L. Sugar, M. Haider, A. Boyes, M. Musquera, M. Bronskill, L. Klotz, *Urology* **2010**, *76*, 1506.

70. B. Du, S. Han, H. Li, F. Zhao, X. Su, X. Cao X, Z. Zhang, *Nanoscale* **2015**, *12*, 5411.

71. M. Amrahli, M. Centelles, P. Cressey, M. Prusevicius, W. Gedroyc, X.-Y. Xu, P.-W. So, *Nanotheranostics* **2021**, *5*, 125.

72. M.-A. Santos, S.-K. Wu, M. Regenold, C. Allen, D.-E. Goertz, K. Hynynen, *Sci. Adv.* **2020**, *6*, 5684.

73. X. Li, J. Kim, J. Yoon, X. Chen, *Adv. Mater.* **2017**, *29*, 23.

74. J.-R. Melamed, R.-S. Edelstein, E.-S. Day, *ACS Nano.* **2015**, *27*, 6.

75. Y. Yang, L. Jing, X. Li, L. Lin, X. Yue, Z. Dai, *Theranostics* **2017**, *6*, 466.

76. O.-U. Akakuru, C. Xu, C. Liu, Z. Li, J. Xing, C. Pan, Y. Li, E.-I. Nosike, Z. Zhang, Z.-M. Iqbal, J. Zheng, A. Wu, *ACS Nano.* **2021**, *15*, 3079.

77. X. Zhang, Y. Li, M. Wei, C. Liu, T. Yu, J. Yang, *Drug Deliv.* **2019**, *26*, 129.

78. M. Wu, Q. Wang, D. Zhang, N. Liao, L. Wu, A. Huang, X. Liu, *Colloids Surf. B Biointerfaces* **2016**, *141*, 467.

79. Y. Wu, Y. Huang, C. Tu, F. Wu, G. Tong, Y. Su, L. Xu, X. Zhang, S. Xiong, X. Zhu, *Nanoscale* **2021**, *13*, p6439–6446.

80. J. Beik, M. Asadi, S. Khoei, S. Laurent, Z. Abed, M. Mirrahimi, A. Farashahi, R. Hashemian, H. Ghaznavi, A. Shakeri-Zadeh, *J. Photochem. Photobiol. B* **2019**, *199*, 111599.

81. M. Wang, Y. Liang, Z. Zhang, G. Ren, Y. Liu, S. Wu, J. Shen, *Anal. Chim. Acta.* **2019**, *1086*, 122.

82. M.-F. Tsai, C. Hsu, C.-S. Yeh, Y.-J. Hsiao, C.-H. Su, L.-F. Wang, *ACS Appl. Mater. Interfaces* **2018**, *10*, 1508.

83. W. Cai, H. Gao, C. Chu, X. Wang, J. Wang, P. Zhang, G. Lin, W. Li, G. Liu, X. Chen, *ACS Appl. Mater. Interfaces* **2017**, *9*, 2040.

84. L. Deng, X. Cai, D. Sheng, Y. Yang, E.-M. Strohm, Z. Wang, H. Ran, D. Wang, Y. Zheng, P. Li, T. Shang, Y. Ling, F. Wang, Y. Sun, *Theranostics* **2017**, *7*, 4410.

85. H. Peng, J. Tang, R. Zheng, G. Guo, A. Dong, Y. Wang, W. Yang, *Adv. Healthc. Mater.* **2017**, *6*, 7.

86. Y. Liu, W. Zhen, Y. Wang, J. Liu, L. Jin, T. Zhang, S. Zhang, Y. Zhao, S. Song, C. Li, J. Zhu, Y. Yang, H. Zhang, *Angew. Chem. Int. Ed. Engl.* **2019**, *58*, 2407.

87. R.-J. Griffin, P.-M. Corry, *Int. J. Hyperthermia* **2009**, *25*, 96.

88. A.-K. Hauser, M.-I. Mitov, E.-F. Daley, R.-C. McGarry, K.-W. Anderson, J.-Z. Hilt, *Biomaterials* **2016**, *105*, 127.

89. E.-J. Moon, P. Sonveaux, P.-E. Porporato, P. Danhier, B. Gallez, I. Batinic-Haberle, Y.-C. Nien, T. Schroeder, M.-W. Dewhirst, *Proc. Natl. Acad. Sci.* **2010**, *107*, 20477.

90. K. Qiu, J. Wang, T.-W. Rees, L. Ji, Q. Zhang, H. Chao, *Chem. Commun.* **2018**, *54*, 14108.

91. Y. Wang, Q. Huang, X. He, H. Chen, Y. Zou, Y. Li, K. Lin, X. Cai, J. Xiao, Q. Zhang, Y. Cheng, *Biomaterials* **2018**, *183*, 10.

92. L. Huang, Y. Li, Y. Du, Y. Zhang, X. Wang, Y. Ding, X. Yang, F. Meng, J. Tu, L. Luo, C. Sun, *Nat. Commun.* **2019**, *10*, 4871.

93. Z. Li, Y. Chen, Y. Yang, Y. Yu, Y. Zhang, D. Zhu, X. Yu, X. Ouyang, Z. Xie, Y. Zhao, L. Li, *Front Bioeng. Biotechnol.* **2019**, *7*, 293.

94. K. Han, Z. Ma, H. Han, *J. Mater. Chem. B* **2018**, *6*, 25.

95. F. Lin, Y.-W. Bao, F.-G. Wu, *Molecules* **2018**, *23*, 3016.

96. Q. Chen, X. Wang, C. Wang, L. Feng, Y. Li, Z. Liu, *ACS Nano* **2015**, *9*, 5223.

97. J. Liao, X. Wei, B. Ran, J. Peng, Y. Qu, Z. Qian, *Nanoscale* **2017**, *9*, 2479.

98. K.-C. Liu, A. Arivajiagane, S.-J. Wu, S.-C. Tzou, C.-Y. Chen, Y.-M. Wang, *Nanomedicine* **2019**, *15*, 285.

99. J. Li, X. Li, S. Gong, C. Zhang, C. Qian, H. Qiao, M. Sun, *Nano Lett.* **2020**, *20*, 4842.

100. Z. Ding, P. Liu, D. Hu, Z. Sheng, H. Yi, G. Gao, Y. Wu, P. Zhang, S. Ling, L. Cai, *Biomater. Sci.* **2017**, *5*, 762.

101. X.-L. Tang, J. Wu, B.-L. Lin, S. Cui, H.-M. Liu, R.-T. Yu, X.-D. Shen, T.-W. Wang, W. Xia, *Acta Biomater.* **2018**, *74*, 360.

102. D. Wang, N. Zhang, X. Jing, Y. Zhang, Y. Xu, L. Meng, *J. Mater. Chem. B* **2020**, *8*, 8271.

103. B. Guo, J. Zhao, Z. Zhang, X. An, M. Huang, S. Wang, *Chem. Eng. J.* **2020**, *391*, 123609.

104. Q. Wu, G. Chen, K. Gong, J. Wang, X. Ge, X. Liu, S. Guo, F. Wang, *Matter* **2019**, *1*, 496.

105. X. Lin, Y. Cao, Y. Xue, F. Wu, F. Yu, M. Wu, X. Zhu, *Nanotechnology* **2020**, *31*, 135101.

106. Q. Feng, Y. Zhang, W. Zhang, Y. Hao, Y. Wang, H. Zhang, L. Hou, Z. Zhang, *Acta Biomater.* **2017**, *49*, 402.

107. A.-M. Gazestani, S. Khoei, S. Khoee, S.-E. Minaei, M. Motevalian, *Artif. Cells Nanomed. Biotechnol.* **2018**, *46*, 25.

108. S.-V. Spirou, M. Basini, A. Lascialfari, C. Sangregorio, C. Innocenti, *Nanomaterials (Basel)* **2018**, *8*, 401.

109. M. Li, W. Bu, J. Ren, J. Li, L. Deng, M. Gao, X. Gao, P. Wang, *Theranostics* **2018**, *8*, 693

110. A. Manigandan, V. Handi, N.-S. Sundaramoorthy, R. Dhandapani, J. Radhakrishnan, S. Sethuraman, A. Subramanian, *Bioconjugate Chem.* **2018**, *29*, 275–286

111. A.-C. Garrido-Castro, N.-U. Lin, K. Polyak, *Cancer Discov.* **2019**, *9*, 176.

AUTHOR BIOGRAPHIES

Ziwei Zhang received her BS degree (2012) in pharmaceutical science and MS degree (2014) in pharmaceutical analysis from Peking University. She then obtained an MSc degree in drug discovery and development at UCL in 2017. She is now a third year PhD student at the UCL School of Pharmacy, working in Gareth's group. Her research interests focus on hybrids of inorganic and polymer materials for MRI-based theranostics.

Gareth R. Williams is a professor of pharmaceutical materials science and head of pharmaceutics in the UCL School of Pharmacy. He was educated at the University of Oxford, and then worked in science programme management and as a postdoctoral researcher before obtaining his first independent academic appointment at London Metropolitan University in 2010. He moved to UCL in 2012 as a lecturer and was promoted to associate professor in 2016 and full professor in 2020. Gareth's research interests focus on the use of inorganic and polymer-based nanomaterials in biomedicine, as well as in the development of advanced analytical techniques.